Mat. Res. Soc. Symp. Proc. Vol. 758 © 2003 Materials Research Society LL1.9

Surface Over-Melt During Laser Polishing of Indirect-SLS Metal Parts

J. A. Ramos[†], D. L. Bourell, J. J. Beaman
Texas Materials Institute, Department of Mechanical Engineering, The University of Texas at Austin
[†]Department of Mechanical and Metallurgical Engineering, Pontificia Universidad Católica de Chile

ABSTRACT

Laser polishing of indirect-SLS parts made from 420 stainless powder infiltrated with bronze has been achieved using CO_2 and Nd:YAG lasers. Two mechanisms have been previously proposed for the reduction in surface roughness, namely: shallow surface melting (SMM) and surface over-melt (SOM). In SMM reflow of the molten surface minimizes the peak-valley height driven by capillary pressure and liquid curvature. On the other hand, during SOM the melting depth is such that the entire surface becomes liquid and formation of surface periodical structures dominates driven by a surface tension gradient. This surface morphology was identified by means of optical and scanning electron microscopy (SEM). The onset of this regime is dictated by the energy density (i.e., ratio of laser power to scan speed and beam diameter) as well as the initial roughness R_a value prior to laser surface polishing. In contrast with SMM, onset of the latter mechanism increases the roughness R_a with speed reduction. A thermo-physical model is presented, signaling good agreement with roughness R_a and characteristic surface wavelength results obtained for varying laser beam scan speeds. Understanding the surface over-melt mechanism is critical for determining the optimum polishing conditions that minimize roughness.

INTRODUCTION

Rapid Prototyping has proven to be a successful technique in shortening the manufacturing cycle for parts with complex geometry [1,2]. Selective Laser Sintering (SLS) is one such RP technology that benefits from the advantage of building up solid object from polymer, ceramic and metal-alloyed materials in powder form [1-3]. To build objects out of metal alloys, two variations of the SLS are currently available, namely, indirect and direct SLS. The former requires post-infiltration of a SLS formed green part (high melting point metal) by metal of low fusion point. The latter technique, as its name indicates, involves consolidation of metal powder by direct laser induced local fusion. However, the surface roughness achieved during the manufacture of rapid prototyping articles by these SLS techniques is still in the range of several microns [3]. At the same time, a sub-micron surface roughness R_a value is determinant when functional mechanical parts are to be built [3,4]. This is an issue yet to be solved along the path of rapid manufacturing evolution. An intermediate step in solving this problem is to employ the hardware available to the SLS process, specifically a high power laser unit and galvanometer scanner mirrors, to provide for laser polishing of the rapid prototyped object. Pursuing this objective, Ramos et al [5] were able to obtain decrements in R_a values up to 3 times the as-received values on indirect-SLS parts made from LaserForm ST-100, an alloy system commercialized by 3D Systems, Inc. This alloy consists of a 420 stainless steel matrix, 40 wt.% infiltrated with bronze (5 wt.% tin). For the operating window used (laser power 320 W and scan speed 692.7-101.3 mm/s), two surface modification regimes existed: shallow surface melting (SMM) and surface over-melt (SOM). In SMM reflow of the molten surface minimizes the peak-valley height driven by capillary pressure and liquid

curvature [6]. On the other hand, during SOM the extent of melting is such that the entire surface becomes liquid and low frequency high amplitude surface periodic formation dominates. These morphologies were identified by means of optical and scanning electron microscopy (SEM) [5,7]. The onset of each regime is dictated by the energy density (i.e., ratio of laser power to scan speed and beam diameter) as well as the initial roughness R_a value prior to laser surface polishing. For a fixed laser power, SMM shows a reduction in roughness R_a below the initial value with decreasing scanning speed up to a limiting value. Further decrease in scan speed causes onset of the SOM mechanism with increase in roughness R_a with speed reduction [5]. The present paper deals with the physical phenomena occurring during the laser surface polishing of indirect-SLS metallic parts, specifically the surface over-melt mechanism as reported in [5,7].

Since high power lasers have been used in materials processing research, observation of regularly spaced striations on metal surfaces after laser induced melting has already been reported [8-10]. The physical properties of the material as well as the laser process condition (i.e., power and speed) appear to determine the formation of such surface periodical structures. In some instances, these surface waves are attributed to an electrodynamic effect caused by the interaction of the laser radiation with surface electromagnetic waves causing modulation of the energy absorbed into the metal [8]. These resonant periodic structures have periods determined by the wavelength polarization and incident angle of the laser radiation [8]. However, experimental data reported in [9] showed that the typical length of these structures for carbon steels is of the order of 400 to 500 microns. Under these circumstances it has been concluded that it is most likely that these "large" wavelength features are not a consequence of the electrodynamic effect only, but are also impacted by the generation and relaxation of thermo-capillary oscillations on the molten surface layer by surface tension gradients induced during the motion of the laser beam. The periodic structures formed this way become frozen before relaxing completely as the cessation of the heat input from the energy source causes fast quenching of the melt [8-10].

A schematic drawing of the laser polishing process utilized to reduce the surface roughness of LaserForm ST-100 indirect SLS parts is illustrated in Figure 1. A focused laser beam of sufficient power to melt the surface of the object was raster-scanned at high speed a long a rectangular track. As shown in Figure 2 the motion of the beam caused the molten material underneath it to be pulled away towards the solidifying front, thus a ripple is formed.

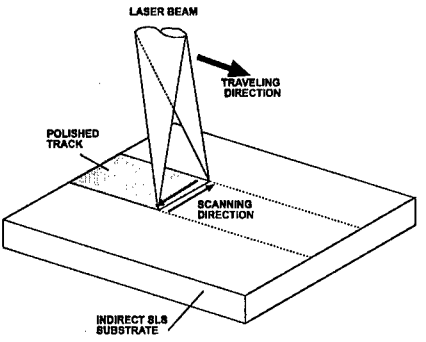

Figure 1. Schematic diagram of the laser polishing process.

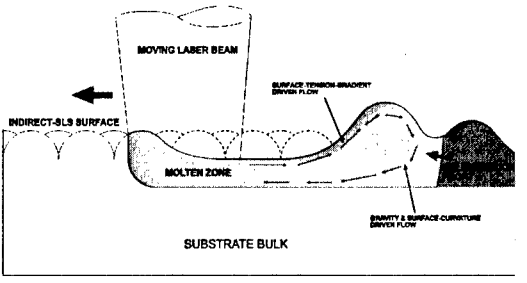

Figure 2. Schematic of a surface periodic structure formation during SOM mechanism.

This mass flow phenomenon is driven by the surface temperature difference between the laser beam and the solidifying zone caused by the motion of the laser beam [8]. This temperature difference creates a surface tension gradient of different sign that exerts a shear force on the liquid surface towards the solidifying front. Gravity and surface curvature effects counter this external shear force.

Once the thermal gradient vanishes, these forces will restore the surface height to the free level. However, viscous forces will delay this relaxation process. The periodic structure thus formed will only relax until the solidification front freezes it [9], assuming that the time for solidification is small relative to the time required for complete relaxation.

The thermo-physical model presented in this paper describes the amplitude behavior of the observed surface micro-relief and estimates the resulting surface roughness R_a. It is assumed that the surface relief formed acquires the shape of a sinusoid of fixed propagation vector, k and spatial phase ϕ. R_a values were measured from laser polished tracks that showed an increment in roughness with reducing scan speed above the as-received value, as well as the characteristic surface wavelength of each track λ. These measurements provided data to validate the model.

THEORY

Thermo-Physical modeling

Figure 3 illustrates a schematic diagram of the different variables that are involved in the formation of a surface relief Δh whenever a laser beam traverses the surface of the material causing a depth of melt h.

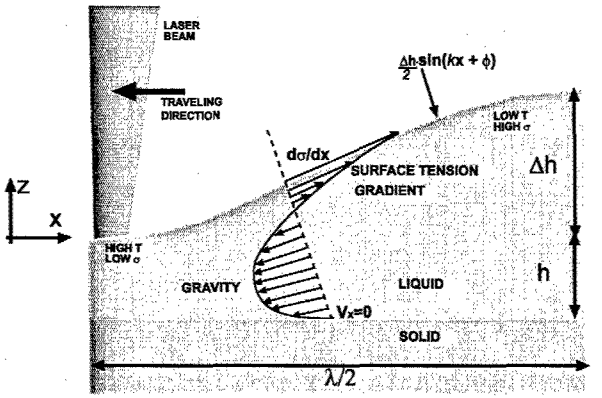

Figure 3. Schematic of the rippling phenomenon encountered in the SOM mechanism.

Anthony and Cline [8] modeled analytically this surface-rippling phenomenon observed during laser surface melting of metals. The steady-state form of the Navier-Stokes equation (i.e., Newton's Second law) for an incompressible fluid in two dimensions (x, z) over a horizontal surface was solved analytically together with the continuity equation, Eq. 1 and 2. Fluctuations in the fluid velocity v_x were considered only in the z direction.

$$-\frac{\partial p}{\partial x}+\frac{\partial}{\partial z}\left(\mu\frac{\partial v_x}{\partial z}\right)=0 \tag{1}$$

$$\int_{-h}^{\Delta h} v_x dz = 0 \tag{2}$$

Where p is the pressure tensor and μ is the dynamic viscosity of the fluid. The main assumption is that the only restoring force acting on the fluid comes from the hydrostatic pressure head difference along the x direction. In other words the effect of gravity g was accounted for as a pressure gradient due to the increase in surface height. This yields,

$$\frac{\partial p}{\partial x}=\rho g\frac{\partial z}{\partial x}\bigg|_{z=\Delta h} \tag{3}$$

Boundary conditions include the existence of a surface tension gradient at the surface of the fluid caused by the surface temperature difference at the laser beam center and where the solidification front is located. A zero velocity in the x direction is also assumed at the solid-liquid interface.

$$\text{at } z = \Delta h \qquad \frac{\partial\sigma}{\partial x}=\mu\frac{\partial v_x}{\partial z}=\frac{\partial\sigma}{\partial T}\frac{dT}{dx} \tag{4}$$

$$\text{at } z = -h \qquad v_x = 0 \tag{5}$$

Where T, σ and ρ are the surface temperature, surface tension and density, respectively. For most metals the surface tension of the liquid phase decreases with increasing temperature, this exerts a shear force that pulls the liquid away from the laser beam center (maximum temperature) towards the solidified zone (minimum temperature) thus forming a surface wave of maximum height, Δh. The expression for this maximum height as presented in [8] is,

$$\Delta h_{MAX}=\frac{3}{2}\cdot\frac{\Delta T}{\rho g h}\cdot\frac{d\sigma}{dT} \tag{6}$$

This expression determines the maximum surface height achieved. This height varies directly with the surface temperature change ΔT between the laser beam and solidification front (i.e., T_L-T_m) and surface tension temperature coefficient. It also varies inversely with the depth of melt h and the gravity term, ρg. There is no term that incorporates the effects of the surface curvature on the formation of the maximum height. We propose the following modification to Eq. 3 and 6, considering that the surface attains a sinusoidal shape having a characteristic wavelength λ. This is,

$$\frac{\partial p}{\partial x}=\left(\rho g\frac{\partial z}{\partial x}+\sigma\frac{\partial^3 z}{\partial x^3}\right)_{z=\Delta h} \tag{7}$$

$$\Delta h_{MAX}=\frac{3}{2}\cdot\frac{\Delta T}{(\rho g+\sigma\left(\frac{2\pi}{\lambda}\right)^2)h}\cdot\frac{d\sigma}{dT} \qquad (8)$$

In this situation gravity and surface curvature provide restoring forces that act against the effect of the surface tension gradient during the laser interaction. Once the laser beam has moved a considerable distance away (greater than λ 2), the surface thermal gradient vanishes and the established periodic surface wave commences to relax driven by these restoring forces (i.e., gravity and curvature). Opposing these forces is the deviatoric component of the pressure tensor of the fluid, namely the viscous force which is proportional to the dynamic viscosity μ of the fluid and the velocity gradient. An expression for the relaxation of the surface height as a function of time t, for times less than the local solidification time of the melt is given by,

$$\Delta h(t)=\Delta h_{MAX}\cdot\exp\left(-\frac{\mu}{\rho}\cdot\left(\frac{2\pi}{\lambda}\right)^2\cdot t\right) \qquad (9)$$

It can be readily shown that the decaying exponential term is typical of an over damped harmonic oscillatory system, and it has been also reported before in [9].

To determine the surface temperature change due to a moving laser beam we resort to the known steady-state analytical solution to the semi-infinite temperature field for a concentrated energy source moving with constant velocity [11]:

$$T(x,y,z)=\frac{P\cdot(1-\Re)}{2\pi\cdot K_{MOD}}\cdot\frac{1}{\sqrt{x^2+y^2+z^2}}\exp\left(-\frac{v_{SCAN}}{2\alpha}\cdot\left(\sqrt{x^2+y^2+z^2}+x\right)\right)+T_0 \qquad (10)$$

Where P, $\Re$, v_{scan}, α, and K_{MOD} have been defined in Table I. As it can be noticed, this expression becomes infinite when evaluated at x = y = z = 0, i.e. immediately below the laser beam. However, distances 1% of the laser beam diameter away from the center of the laser beam give a compromise for evaluating the surface temperature beneath the laser, T_L.

At the same time, Eq. 10 serves the purpose of estimating a value of the depth of melt, h. Although this expression does not consider the phase change from solid to liquid when the temperature field reaches the melting point, this effect can be approximated by modifying the heat conductivity, K, such that it includes the latent heat of fusion of the material [12].

Obtaining the maximum depth of melt means finding the coordinates (x_{max}, z_{max}) for y = 0 from Eq. 10. The maximum depth of melt , z_{max} = -h, occurs at half the length value of the major axis of the surface isothermal ellipse (i.e., at $T=T_m$). By making y = 0 and z = 0, and solving Eq. 10 for x, two values are found, and x_{max} is the average of the latter two roots. Then, z_{max} is found by solving Eq. 10 again this time evaluating it at y = 0 and x = x_{max}, and the negative root corresponds to h. Equation 10 also can provide a way to determine the solidification time, since the heat flow at the maximum depth of melt can be determined from it. This is obtained by taking the first derivative with respect to z, and evaluating it at (x_{max}, 0, z_{max}). The average solidification front velocity at the maximum depth of melt can be then obtained by using the Stefan condition [13], taking into account the specific latent heat of solidification of the alloy, L.

$$\bar{v}_{SOLIDIFICATION} = \frac{-K \left.\frac{\partial T}{\partial z}\right|_{z=-h}}{\rho L} \quad (11)$$

This velocity can then be used to estimate the average solidification time,

$$t_{SOLIDIFICATION} = \frac{2h}{\bar{v}_{SOLIDIFICATION}} \quad (12)$$

Finally, the estimation of the average arithmetic surface roughness R_a can be assessed simply by evaluating half of the maximum height after a relaxation time equal to $t_{SOLIDIFICATION}$, this is,

$$R_a = \frac{\Delta h(t_{SOLIDICATION})}{2} \quad (13)$$

RESULTS AND DISCUSSION

Optical and SEM observations

Figure 4 shows an optical macrograph of the surface of a laser polishing track created using a 320 W laser and a scanning speed of 128.9 mm/s, (620.6. J/cm^2). The average width of this track is 1930 μm. A periodic pattern of oblique linear features can be observed forming an angle of 30° with the horizontal axis (i.e., the laser beam scanning direction). From SEM observation at low magnification of the same sample surface, it can be seen more clearly that this periodic pattern is spaced in average every 360 μm approximately, Figure 5.

Figure 6 shows a higher magnification SEM image of the surface of the same laser track illustrating two consecutive pattern peaks which are spaced apart a magnitude λ = 300 μm and are clearly parallel to each other. Another feature seen on this image is the appearance of a second periodic pattern closely spaced making a 30° angle with the former. This pattern however, seems discontinuous by comparison.

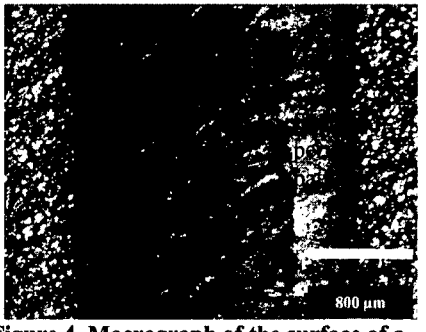

Figure 4. Macrograph of the surface of a SOM laser polished track, x25.

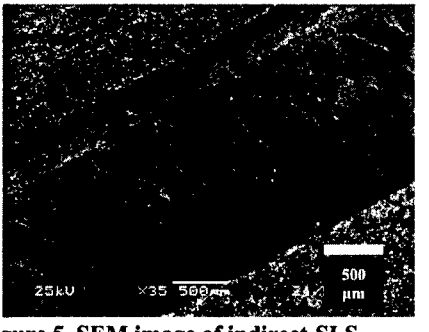

Figure 5. SEM image of indirect-SLS surface treated under SOM conditions, x35.

Closer examination of the surface in Figure 7 reveals that the second periodic pattern is dispersed, yet it has a shorter spacing of 10-20 μm. It is also perpendicular to the traveling direction of the laser beam thus parallel to the scanning direction. It consists of multiple agglomerated particles (1-5 μm in size), most likely oxides of Si, Al and Cr as determined previously [6].

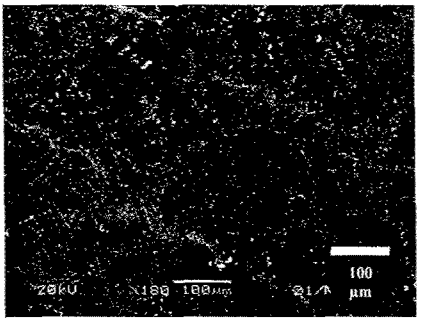

Figure 6. SEM image showing two consecutive periodic peaks, x180.

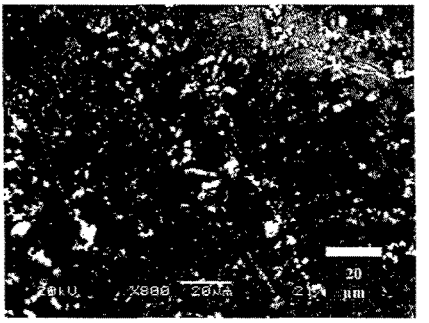

Figure 7. SEM image illustrating oxide particles along high frequency ripples, x800.

Thermo-Physical model results

The results of the thermo-physical model described previously are plotted in Figure 8 as surface roughness data together with experimental data measured from several laser polished tracks performed on LaserForm-ST100 specimens. The as-received R_a value of the surface was 2.98 μm. The laser power was kept fixed at 320 W and the scanning speed was varied from 692.7 to 101.3 mm/s. However, only the R_a results for speeds ranging from 177.2 to 101.3 mm/s are plotted below, as this is thought to be part of the SOM regime. Table I presents the variables included in the model as well as their values and units. Physical properties correspond to a 60 wt.% 420 stainless steel - 40 wt.% bronze (5 wt.% tin) alloy mixture.

Table I. Definition of variables.

Variable	Definition	Value
P	Laser power	320 W
R	Reflective and convective loses	0.725
ρ	Density of solid phase	8247 kg/m^3
α	Thermal diffusivity of solid phase	$4.985 \cdot 10^{-5}$ m^2/s
L	Specific latent heat of solidification	146500 J/kg
K	Heat conductivity of solid	172 W/m/K
K_{MOD}	Modified heat conductivity	216 W/m/K
v_{SCAN}	Laser beam scan speed	101-177 mm/s
T_M	Melting temperature	1347 °C
To	Initial temperature	25°C
μ	Viscosity of the liquid	5.45 mPa/s
σ	Surface tension of liquid-vapor	1.609 J/m^2
dσ/dT	Surface tension temperature coefficient	-26.1 mJ/m^2

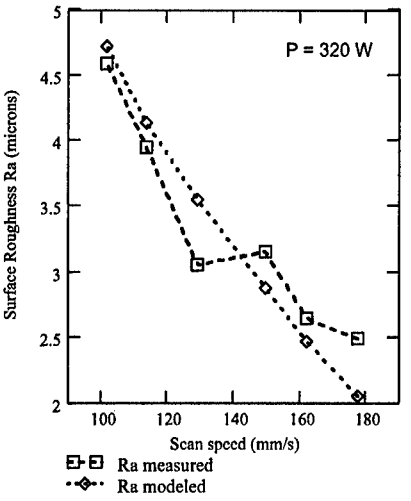

Figure 8. Plot of experimental and modeled surface roughness R_a data versus scan speed.

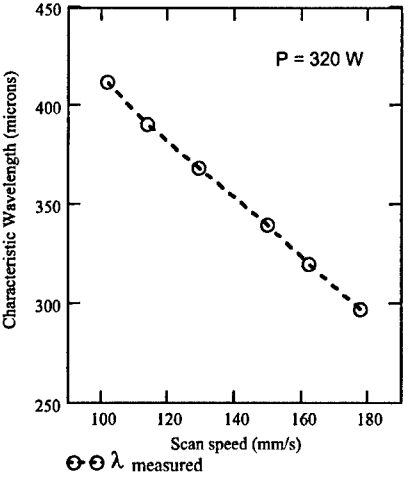

Figure 9. Plot of the measured average surface wavelength λ versus scan speed.

From the plot in Figure 8 it can be seen that the experimental data show an increment in the R_a value with decreasing scan speed. Only the data point corresponding to a scan speed of 128.9 mm/s seems to be lower compared to its predecessor. Nonetheless the difference in 0.10 μm falls within the standard deviation of the measurements (i.e., +-0.69 μm). The modeled R_a value shows the same trend as the measured values within the same order of magnitude. From the model, it can be inferred that as the scan speed is lowered the surface temperature immediately under the center of the laser beam increases, increasing the amplitude of the surface wave, but simultaneously the depth of melt is increased and so is the solidification time. These latter two variables tend to decrease the relief amplitude, however the effect of temperature overwhelms them. Moreover, the effect of adding a surface curvature term brings the amplitude down to a reasonable order of magnitude. The latter term and the viscous damping term depend on the characteristic wavelength of the surface periodic structure solidified. A plot of the measured average characteristic wavelength λ for each laser track is presented in Figure 9. Its trend is much the same as that of the modeled R_a values. We can infer that this parameter plays a significant role in the determination of the amplitude of the surface relief. As for the second periodic pattern observed under the SEM (Figs. 6 and 7), this model does not take into account its additive effect on the modeled surface roughness. However, it can be considered as part of the noise when measuring the R_a value of the treated surfaces experimentally.

CONCLUSIONS

Optical and SEM observation of the surface of the laser polished tracks under the SOM regime confirm the formation of two periodical structures, one of high frequency low amplitude and the other of low frequency high amplitude. Both contribute to the surface roughness

achieved after the laser polishing process, but the latter is thought to be more critical in increasing the R_a value above the as-received level.

A modified thermo-physical model based on previously reported models [8,9] is presented, signaling good agreement with roughness R_a and characteristic surface wavelength results obtained for a fixed laser power and varying laser beam scan speeds. Increment in roughness R_a value with decreasing scanning speed is predicted by the present model. The main contribution of the present model is the incorporation of the surface curvature effects as a restoring force aiding gravity to bring the amplitude of the surface wave down to zero. The main assumption here is that the surface relief behaves as it if were a sinusoid of fixed propagation vector.

ACKNOWLEDGEMENTS

The Laboratory for Freeform Fabrication gratefully acknowledges the support of the Office of Naval Research for funding the project "Surface Engineering for SFF Processes", Grant N°: N00014-00-1-0334. We would also like to thanks 3D Systems, Inc. (former DTM Corporation) for providing LaserForm™ ST-100 samples for testing.

REFERENCES

1. J.J.Beaman, J.W.Barlow, D.L.Bourell, and R.H.Crawford, *Solid Freeform Fabrication: A New Direction in Manufacturing,* (Kluwer Academic 1997).
2. J.A. McDonald, C.J. Ryall and D.I. Wimpenny, *Rapid Prototyping Casebook*, (Professional Engineering Publishing 2001).
3. L. Lü, J. Fuh and Y.S. Wong, *Laser Induced Materials and Processes for Rapid Prototyping*, (Kluwer Academic 2001).
4. J. Connolly, Direct Rapid Manufacturing – Is it Possible?, *Time Compression Technologies*, May (2001), pp. 46-47.
5. J.A.Ramos, J. Murphy, K.Wood, D.L. Bourell and J.J. Beaman, Surface Roughness Enhancement of Indirect-SLS Metal Parts by Laser Surface Polishing, *SFF Symposium Proc.*, 12 (2001).
6. J.A. Ramos and D.L. Bourell, in *Rapid Prototyping of Materials*, edited by F.D.S. Marquis and D.L. Bourell, (TMS, Warrendale PA, 2002), pp. 191-201.
7. J.A. Ramos, D.L. Bourell, and J.J. Beaman, Surface Characterization of Laser Polished Indirect-SLS Parts, *SFF Symposium Proc.*, 13 (2002).
8. A.M. Prokhorov, V.I.Konov, I. Ursu and I.N.Mihăilescu, *Laser Heating of Metals,* (Adam Hilger, 1990) pp.115-124.
9. T.R. Anthony and H.E. Cline, *J. Applied Physics*, Vol. 48, No 9, 3888-3894 (1977).
10. V.S. Avanesov and M.A. Zuev, "Investigation of surface topography after melting by laser beam", SPIE, Vol. 2713, 340-343.
11. D. Rosenthal, *Trans. ASME*, Vol. 68, 849-865 (1946).
12. Ø. Grong, N. Christensen, *J. Mater. Sci. and Tech.*, Vol. 2, 967-973 (1986).
13. W. Kurz, D.J. Fisher, *Fundamentals of Solidification,* 4th ed. (Trans Tech Publications, Zuerich, 1998) p. 164.

Solution and Spray Processing